Thermodynamics of spinless fermion on triangular plaquettes or tetrahedral chain

M. Rojas, S. M. de Souza and Onofre Rojas
Departamento de Ciências Exatas, Universidade Federal de Lavras. C.P. 3037, 37200-000, Lavras - MG, Brazil.

The spinless fermion on triangular plaquettes or tetrahedral chain is considered in this work with hooping term, repulsive Coulomb interactions between nearest-neighbor sites and chemical potential. This is an exactly solvable model, through decoration transformation and transfer matrix approach, when the hopping term acting with nodal sites is ignored, but all other parameters considered are quite general. Five different states are shown in the phase diagrams, these states are distinguished by particle density, empty, 1, 2, 3 and 4 particles per unit cell on the triangular plaquette and one nodal site, or a tetrahedron unit cell. The boundary of these regions are frustrated state curves. The phase with particle density 2 is limited by a frustrated state curve with non-trivial residual entropy, whereas the other boundaries are limited also by frustrated state curves, but with trivial residual entropy. The existence of this non-trivial phenomenon has also been evidenced by temperature dependencies of the specific heat. The behavior of the specific heat at low-temperature is influenced by the interaction between thermal and quantum fluctuations. Finally some other additional quantities were also considered, such as the internal energy and compressibility.

I. INTRODUCTION

The Hubbard model was introduced to describe the correlation of electrons in the narrow band of transition metals. By extending the model and changing the parameters, it is possible that the Hubbard model could describe many properties of strongly correlated electron system. Montenegro-Filho and Coutinho-Filho [1] considered the doped AB2 Hubbard chain, both in the weak coupling and the infinite-U limit (atomic limit). They studied a quite interesting phase as a function of hole doping away from half-filled band. In fact, in several works, many properties of the system are presented as a function of the chemical potential μ. Although from a theoretical point of view the chemical potential and particle density are conjugated variables, experimentally, it is possible to manipulate in a controlled way, by varying the entering and outgoing particles to the system. Mancini [2] has presented the exact solution of extended one-dimensional Hubbard model in the atomic limit, obtaining the chemical potential plateaus of the particle density, of the on-site potential at zero temperature and studied the thermodynamic charge susceptibility, and the compressibility at finite temperature, as well as other physical quantities. Vidal *et al.* [3] also discussed two interacting particles evolving in a diamond chain structure embedded in a magnetic field. As the particles interact, it leads to the strong localization induced by the magnetic field for the particular value of a flux. Analogous model was also studied by Rossler and Mainemer [4]. The Hubbard model in other quasi one-dimensional triangular structure also was studied by Wang [5]. The latter indicated that for small hopping term, the system exhibits short range antiferromagnetic correlation, whereas, when the hopping terms become greater than the critical point, there is a transition from an antiferromagnetic state to a frustrated one. Moreover, the insulator-metal transition takes place at hopping interaction even greater than another critical point. Further Gulacsi *et al.* [6, 7] also discussed the diamond Hubbard chain in a magnetic field and a wide range of properties such as flat-band ferromagnetism and the correlation induced metallic, half-metallic process.

In the last decade several diamond chain structures were discussed. Some of them were motivated by real materials such as Cu3(CO3)2(OH)2 known as azurite, which is an interesting quantum antiferromagnetic model, described by Heisenberg model on generalized diamond chain. Honecker *et al.* [8] studied the dynamic and thermodynamic properties for this model. Besides, Pereira *et al.* [9] investigated the magnetization plateau of delocalized interstitial spins on diamond chain, they also detected magnetocaloric effect in kinetically frustrated diamond chain. Moreover, the thermodynamics of the Ising-Heisenberg model on diamond-like chain was widely discussed in Refs. [10–13], and also the thermal entanglement of this structure was considered [14]. Recently, Lisnii [15] studied a distorted diamond Ising-Hubbard chain and that model also exhibits geometrical frustration. The spinless versions of the Hubbard model on diamond chain was also recently investigated through exact analytical solution [16], Lopes and Dias [17] performed a detailed investigation using the exact diagonalization approach. The extended Hubbard model on diamond chain structure [18] also can be solved exactly in quasi-atomic limit, and this model exhibits a quite reach phase diagram at zero temperature, the thermodynamics also exhibits very remarkable properties due to the influence of geometric frustration.

On the other hand, coupled tetrahedral chain structure was first introduced by Mambrini *et al.* [19] to discuss the residual entropy and spin gap in tetrahedral coupled Heisenberg chain, later Rojas and Alcaraz [20] also discussed a more rigorous result of the tetrahedral Heisenberg chain using numerical approach, the quantum phase transition and geometric frustration of this model, and later Antonosyan *et al.* [21] have studied the exact solution of the Ising-Heisenberg chain with triangular XXZ-Heisenberg plaquettes (or tetrahedral chain) [21, 22]. The Hubbard model version of this structure

also was considered by Batista and Shastry [23], and more recently Maksymenko *et al.* [24] discussed the localized states on triangular trap and low temperature properties of the antiferromagnetic Heisenberg and repulsive Hubbard models.

The outline of this paper is as follows. In Sec. 2, we introduce the model to be studied. In Sec. 3, we present the phase diagram at zero temperature. In Sec. 4 is devoted to the decoration transformation and transfer matrix approach, in order to obtain its exact solution. Whereas in Sec. 5 the thermodynamics properties of the model are discussed. Finally, we summarize our conclusions in Sec. 6.

II. TRIANGULAR PLAQUETTES CHAIN

The one-dimensional lattice of the spinless fermion model on triangular plaquettes [21, 22] or also known as tetrahedral chain [20] is considered, which is schematically illustrated in Fig. 1. From now on, conveniently we will call this structure as the triangular plaquettes chain, thus the total Hamiltonian of the model, can be expressed by

$$H \;=\; \sum_{i=1}^{N} \mathbf{H}_{i,i+1}, \tag{1}$$

where

$$\begin{aligned}\mathbf{H}_{i,i+1} \;=\; & -t\left(\mathbf{a}^{\dagger}_{a,i}\mathbf{a}_{b,i}+\mathbf{a}^{\dagger}_{b,i}\mathbf{a}_{c,i}+\mathbf{a}^{\dagger}_{c,i}\mathbf{a}_{a,i}+h.c.\right)\\ & -\mu\left(\mathbf{n}_{a,i}+\mathbf{n}_{b,i}+\mathbf{n}_{c,i}+\frac{1}{2}(\mathbf{n}_{d,i}+\mathbf{n}_{d,i+1})\right)\\ & +V_1\left(\mathbf{n}_{a,i}\mathbf{n}_{b,i}+\mathbf{n}_{b,i}\mathbf{n}_{c,i}+\mathbf{n}_{c,i}\mathbf{n}_{a,i}\right)\\ & +\frac{V}{2}\left(\mathbf{n}_{d,i}+\mathbf{n}_{d,i+1}\right)\left(\mathbf{n}_{a,i}+\mathbf{n}_{b,i}+\mathbf{n}_{c,i}\right), \end{aligned} \tag{2}$$

and N the number of unit cell; $\mathbf{a}_{\alpha,i}(\mathbf{a}^{\dagger}_{\alpha,i})$ are the Fermi annihilation (creation) operators at the ith site, for spinless (or completely polarized) fermion respectively, with $\alpha=\{a,b,c,d\}$, and $\mathbf{n}_{\alpha,i}$ the number operator defined as $\mathbf{n}_{\alpha,i}=\mathbf{a}^{\dagger}_{\alpha,i}\mathbf{a}_{\alpha,i}$. The hopping parameter t corresponds to the exchange constant of an interstitial spinless particle, μ is the chemical potential and the Coulomb repulsion term between fermions on neighboring sites are represented for V and V_1.

The spinless fermion model on tetrahedron chain, has an important particle-hole symmetry [16, 25]. For the purpose of this discussion, the following canonical transformation $\mathbf{a}^{\dagger}_{\alpha,i}\rightarrow\mathbf{a}_{\alpha,i}$ and $\mathbf{a}_{\alpha,i}\rightarrow\mathbf{a}^{\dagger}_{\alpha,i}$ was considered. For the occupation number operator the transformation reads $\mathbf{n}_{\alpha,i}\rightarrow\mathbf{a}_{\alpha,i}\mathbf{a}^{\dagger}_{\alpha,i}=\mathbf{1}-\mathbf{n}_{\alpha,i}$, thus the transformed Hamiltonian becomes

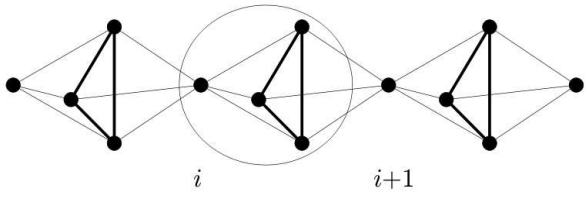

FIG. 1: Squematic representation of spinless fermion model on triangular plaquettes or tetrahedral chain. The bold lines we represent a plaquette with hopping term and Coulomb repulsion between two sites, while by thin lines we represent only the Coulomb repulsion term of nodal particles and particles on plaquette site, at $i-$th site.

$$\begin{aligned}\mathbf{H}'_{i,i+1} \;=\; & t\left(\mathbf{a}^{\dagger}_{a,i}\mathbf{a}_{b,i}+\mathbf{a}^{\dagger}_{b,i}\mathbf{a}_{c,i}+\mathbf{a}^{\dagger}_{c,i}\mathbf{a}_{a,i}+h.c.\right)\\ & +\left(\mu-2V_1-V\right)\left(\mathbf{n}_{a,i}+\mathbf{n}_{b,i}+\mathbf{n}_{c,i}\right)\\ & +\left(\frac{\mu}{2}-\frac{3V}{2}\right)\left(\mathbf{n}_{d,i}+\mathbf{n}_{d,i+1}\right)\\ & +V_1\left(\mathbf{n}_{a,i}\mathbf{n}_{b,i}+\mathbf{n}_{b,i}\mathbf{n}_{c,i}+\mathbf{n}_{c,i}\mathbf{n}_{a,i}\right)\\ & +\frac{V}{2}\left(\mathbf{n}_{d,i}+\mathbf{n}_{d,i+1}\right)\left(\mathbf{n}_{a,i}+\mathbf{n}_{b,i}+\mathbf{n}_{c,i}\right)\\ & +\left(3V-3V_1-4\mu\right). \end{aligned} \tag{3}$$

Alternatively, using the Wigner-Jordan transformation it is possible to map the spinless fermion tetrahedron chain onto an Ising-Heisenberg triangular plaquettes chain, the z-component of the spin-1/2 operator is related to the number operator by $\mathbf{n}=1/2-\sigma^z$, while the creation (annihilation) operators are related through $\mathbf{a}^{\dagger}_j=2^j\left(\prod_{k<j}\sigma^z_k\right)\sigma^-_j$ and $\mathbf{a}_j=2^j\left(\prod_{k<j}\sigma^z_k\right)\sigma^+_j$.

In order to solve this model the first step is to obtain all the eigenvalues and eigenvectors of the Hamiltonian Eq. (2), to evaluate this one, we considered the state vector for the sites a, b and c connected by hopping term t. In each state there are only two possibilities labeled by 0 or 1, that means an empty or occupied particle state respectively.

The states acting on Hamiltonian (2) at sites a, b and c for each elementary cell become

$$\mathbf{H}_{i,i+1}\mid 000\rangle \;=\; -\frac{1}{2}\mu\,\overline{\mathbf{n}}_d\mid 000\rangle, \tag{4}$$

$$\mathbf{H}_{i,i+1}\left\{\begin{array}{c}\mid 100\rangle\\ \mid 010\rangle\\ \mid 001\rangle\end{array}\right\} \;=\; \left\{\begin{array}{c}\boldsymbol{f}_+\\ \boldsymbol{f}_+\boldsymbol{R}\\ \boldsymbol{f}_+\boldsymbol{R}^2\end{array}\right\}\mid 100\rangle, \tag{5}$$

$$\mathbf{H}_{i,i+1}\left\{\begin{array}{c}\mid 110\rangle\\ \mid 011\rangle\\ \mid 101\rangle\end{array}\right\} \;=\; \left\{\begin{array}{c}\boldsymbol{f}_-\\ \boldsymbol{f}_-\boldsymbol{R}\\ \boldsymbol{f}_-\boldsymbol{R}^2\end{array}\right\}\mid 110\rangle, \tag{6}$$

$$\mathbf{H}_{i,i+1}\mid 111\rangle \;=\; \left[2\alpha_- -\alpha_+ +V_1\right]\mid 111\rangle. \tag{7}$$

Hereafter, the following notations are introduced, $\boldsymbol{R}$ represents a cyclic shift operator, $\overline{\mathbf{n}}_d=\mathbf{n}_{d,i}+\mathbf{n}_{d,i+1}$ is the occupation number operator for nodal particles of the triangular plaquettes chain. Finally we define the operator

$\boldsymbol{f}_{\pm} = \alpha_{\pm}\mathbf{1} - t\boldsymbol{R} - t\boldsymbol{R}^2$, where $\alpha_+ = -\mu + \left(\frac{V}{2} - \frac{\mu}{2}\right)\overline{\mathbf{n}}_d$ and $\alpha_- = -2\mu + V_1 + \left(V - \frac{\mu}{2}\right)\overline{\mathbf{n}}_d$.

After diagonalizing the Hamiltonian $\mathbf{H}_{i,i+1}$, we obtain the following eigenvectors

$$
\begin{aligned}
\mid v_0\rangle &= \mid 000\rangle, && (8)\\
\mid v_1\rangle &= \frac{1}{\sqrt{3}}\left(\mathbf{1} + \boldsymbol{R} + \boldsymbol{R}^2\right) \mid 100\rangle, && (9)\\
\mid v_2\rangle &= \frac{\sqrt{6}}{6}\left(-\mathbf{1} - \boldsymbol{R} + \mathbf{2}\boldsymbol{R}^2\right) \mid 100\rangle, && (10)\\
\mid v_3\rangle &= \frac{\sqrt{2}}{2}\left(-\mathbf{1} + \boldsymbol{R}\right) \mid 100\rangle, && (11)\\
\mid v_4\rangle &= \frac{1}{\sqrt{3}}\left(\mathbf{1} + \boldsymbol{R} + \boldsymbol{R}^2\right) \mid 110\rangle, && (12)\\
\mid v_5\rangle &= \frac{\sqrt{6}}{6}\left(-\mathbf{2} + \boldsymbol{R} + \boldsymbol{R}^2\right) \mid 110\rangle, && (13)\\
\mid v_6\rangle &= \frac{\sqrt{2}}{2}\left(\boldsymbol{R} - \boldsymbol{R}^2\right) \mid 110\rangle, && (14)\\
\mid v_7\rangle &= \mid 111\rangle. && (15)
\end{aligned}
$$

The eigenvalues were obtained as a function of the chemical potential μ, nearest neighbor Coulomb coupling V, V_1 and the hopping term t, and the corresponding eigenvalues are

$$
\begin{aligned}
E_0 &= -\frac{\mu}{2}\,\overline{n}_d, && (16)\\
E_1 &= -2t - \mu + \left(-\frac{\mu}{2} + \frac{V}{2}\right)\overline{n}_d, && (17)\\
E_2 = E_3 &= t - \mu + \left(-\frac{\mu}{2} + \frac{V}{2}\right)\overline{n}_d, && (18)\\
E_4 &= -2t + V_1 - 2\mu + \left(-\frac{\mu}{2} + V\right)\overline{n}_d, && (19)\\
E_5 = E_6 &= t + V_1 - 2\mu + \left(-\frac{\mu}{2} + V\right)\overline{n}_d, && (20)\\
E_7 &= -3\mu + 3V_1 + \left(-\frac{\mu}{2} + \frac{3V}{2}\right)\overline{n}_d, && (21)
\end{aligned}
$$

where $\overline{n}_d$ is the eigenvalue of operator $\overline{\mathbf{n}}_d$. The energies $E_2 = E_3$ and $E_5 = E_6$ are twofold degenerate. Furthermore, using the particle-hole symmetry and considering $V_1 = V$, we have the following constraints $\mu = \frac{3V}{2}$, which corresponds to the half-filled band system.

III. GROUND STATE PHASE DIAGRAM

In order to study the phase diagram at $T = 0$, we use the diagonalized version of the Hamiltonian presented in the previous section. The ground state phase diagram for t as a function of μ is displayed in Fig. 2, and for fixed values of $V_1 = V = 1$. In any case, only five ground-state energies were found, which are described as follows

$$
\begin{aligned}
\rho = 0: &\quad E_0 = 0 && \overline{n}_d = 0, && (22)\\
\rho = 1: &\quad E_1 = -2t - \mu, && \overline{n}_d = 0, && (23)\\
\rho = 2: &\quad \begin{cases} E_1 = -2t + 1 - 2\mu, & \overline{n}_d = 2, \\ E_4 = -2t + 1 - 2\mu, & \overline{n}_d = 0, \end{cases} && (24)\\
\rho = 3: &\quad E_4 = -2t + 3 - 3\mu, && \overline{n}_d = 2, && (25)\\
\rho = 4: &\quad E_7 = -4\mu + 6, && \overline{n}_d = 2, && (26)
\end{aligned}
$$

by ρ we denoted the electron density per elementary cell.

Therefore, the corresponding eigenvectors are given by

$$
\begin{aligned}
\mid S0\rangle &= \prod_{i=1}^{N} \mid 000\rangle_i \otimes \mid 0\rangle_i,\ \rho = 0 && (27)\\
\mid S1\rangle &= \prod_{i=1}^{N} (\boldsymbol{g} \mid 100\rangle_i) \otimes \mid 0\rangle_i,\ \rho = 1 && (28)\\
\mid F1\rangle &= \prod_{i=1}^{N} (\boldsymbol{g} \mid 110\rangle_i) \otimes \mid 0\rangle_i,\ \rho = 2 && (29)\\
\mid F2\rangle &= \prod_{i=1}^{N} (\boldsymbol{g} \mid 100\rangle_i) \otimes \mid 1\rangle_i,\ \rho = 2 && (30)\\
\mid S3\rangle &= \prod_{i=1}^{N} (\boldsymbol{g} \mid 110\rangle_i) \otimes \mid 1\rangle_i,\ \rho = 3 && (31)\\
\mid S4\rangle &= \prod_{i=1}^{N} \mid 111\rangle_i \otimes \mid 1\rangle_i,\ \rho = 4\ , && (32)
\end{aligned}
$$

where we define the operator $\boldsymbol{g} = \frac{1}{\sqrt{3}}\left(\mathbf{1} + \boldsymbol{R} + \boldsymbol{R}^2\right)$ and the states of type $\mid a, b, c\rangle \otimes \mid d\rangle$ corresponds to the particles at sites a, b, c and d, respectively in the unit cell.

In Fig. 2, it can be observed that there are five ground states in the phase diagram. These states are limited as follow:

$$
\begin{aligned}
&|S0\rangle: \text{ limited by } \quad \mu \leqslant -2t, \text{ with } \quad \rho = 0, && (33)\\
&|S1\rangle: \text{ in the range } \quad -2t \leqslant \mu \leqslant 1 \quad \text{with} \quad \rho = 1, && (34)\\
&\left\{ \begin{array}{l} |F1\rangle \\ |F2\rangle \end{array} \right\}: \text{ in the range } \quad 1 \leqslant \mu \leqslant 2 \quad \text{with} \quad \rho = 2, && (35)\\
&|S3\rangle: \text{ in the range } \quad 2 \leqslant \mu \leqslant 2t{+}3 \ \text{ with } \quad \rho = 3, && (36)\\
&|S4\rangle: \text{ limited } \quad \mu \geqslant 2t + 3 \quad \text{with} \quad \rho = 4. && (37)
\end{aligned}
$$

The first state is $|S0\rangle$, this corresponds just to a simple empty lattice particle (or fully-filled holes) on triangular plaquettes chain with total density $\rho = 0$. The second one is represented by $|S1\rangle$, where one particle may stay

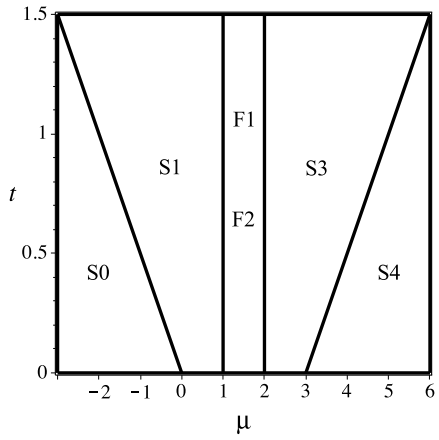

FIG. 2: Ground-state phase diagram of triangular plaquettes chain, as a function μ against t, for $V = V_1 = 1.0$

at a, b or c of the elementary cell, then the particle density for this state is $\rho = 1$. When the density takes the value $\rho = 2$, we have two-fold degenerate states $|F1\rangle$ and $|F2\rangle$, the first degenerate state corresponds to the configuration in which two particles are fluctuating in sites a, b and c. In the second degenerate state $|F2\rangle$, we have only one particle fluctuating at sites a, b and c, whereas on site d of elementary cell there is another particle. In the case of state $|S3\rangle$ ($\rho = 3$), two particles occupy the three interstitial sites a, b and c, in this case, we have one particle in nodal site d. Finally there is a fully-filled particle in triangular plaquettes chain, whose state can represented by $|S4\rangle$ with density $\rho = 4$.

IV. DECORATION TRANSFORMATION

In order to study the thermodynamic properties of the spinless fermion model on triangular plaquettes chain, it will be used the decoration transformation [26–29] as described below. It is not necessary to map the spinless fermion model onto spin models, like Ising-Heisenberg model [11, 12, 30–33]. Thus, there is an interest in performing the decoration transformation for operators. In this sense, it will be applied directly the decoration transformation approach [11, 12, 30–33] for the proposed model. The main aim to solve the Hamiltonian Eq. (1) of spinless fermion model on triangular plaquettes chain is to map onto an effective spinless fermion model without hopping term, whose Hamiltonian is given by

$$\widetilde{\mathbf{H}} = \sum_{i=1}^{N} \left[\widetilde{V} \mathbf{n}_{d,i} \mathbf{n}_{d,i+1} - \frac{\tilde{\mu}}{2} \left(\mathbf{n}_{d,i} + \mathbf{n}_{d,i+1} \right) \right], \qquad (38)$$

where $\widetilde{V}$ and $\tilde{\mu}$ are coefficients to be determined using decoration transformation.

The Boltzmann factor of effective spinless fermion model can be expressed as follows

$$\tilde{w}(\mathbf{n}_{d,i},\, \mathbf{n}_{d,i+1}) = e^{\beta\left(-\tilde{V}\mathbf{n}_{d,i}\mathbf{n}_{d,i+1} + \frac{\tilde{\mu}}{2}(\mathbf{n}_{d,i}+\mathbf{n}_{d,i+1})\right)}, \quad (39)$$

where $\beta = (k_B T)^{-1}$ with k_B as the Boltzmann's constant and T as the absolute temperature. On the other hand, the Boltzmann factors for the spinless fermion model on triangular plaquettes chain is given by the Hamiltonian (1), which reads as

$$w\left(\mathbf{n}_{d,i}, \mathbf{n}_{d,i+1}\right) = tr_{a,b,c}\left(e^{-\beta \mathbf{H}_{i,i+1}}\right), \qquad (40)$$

whereas the operators $\mathbf{n}_{d,i}$ have two eigenvalues 0 and 1 , thus, one obtains from Eq. (40) three different Boltzmann factors, which are written down as

$$\begin{aligned} w\left(0,0\right) &= 1 + e^{\beta(2t+\mu)} + 2e^{\beta(-t+\mu)} + e^{\beta(2t-V_1+2\mu)} + \\ &\quad 2e^{\beta(-t-V_1+2\mu)} + e^{\beta(3\mu-3V_1)}, \qquad (41) \\ w\left(0,1\right) &= e^{\frac{\beta\mu}{2}} + e^{\beta(2t+\frac{3\mu}{2}-\frac{V}{2})} + 2e^{\beta(-t+\frac{3\mu}{2}-\frac{V}{2})} + \\ &\quad e^{\beta(2t-V_1+\frac{5\mu}{2}-V)} + 2e^{\beta(-t-V_1+\frac{5\mu}{2}-V)} + \\ &\quad e^{\beta(\frac{7\mu}{2}-3V_1-\frac{3V}{2})}, \qquad (42) \\ w(1,1) &= e^{\beta\mu} + e^{\beta(2t+2\mu-V)} + 2e^{\beta(-t+2\mu-V)} + \\ &\quad e^{\beta(2t-V_1+3\mu-2V)} + 2e^{\beta(-t-V_1+3\mu-2V)} + \\ &\quad e^{\beta(4\mu-3V_1-3V)}. \qquad (43) \end{aligned}$$

For simplicity, we denote by $w_0 = w(0,0)$, $w_1 = w(1,0) = w(0,1)$ and $w_2 = w(1,1)$. Applying a decoration-interaction transformation, the partition function for the present model, must satisfy the following condition

$$Z(V, V_1, \mu, t, T) = f\, Z_{eff}(\tilde{V}, \tilde{\mu}, T). \qquad (44)$$

The Boltzmann factor for both systems must be equal in order to satisfy the decoration transformation [27, 28]. Thus, there are three unknown algebraic equations and three unknown parameters, this algebraic system is solved easily using the decoration transformation method, whose solutions are written as

$$f = w_0, \quad \tilde{\mu} = \frac{2}{\beta} \ln\left(\frac{w_1}{w_0}\right), \quad \tilde{V} = \frac{1}{\beta} \ln\left(\frac{w_1^2}{w_2 w_0}\right), \quad (45)$$

where the f, $\tilde{\mu}$ and $\tilde{V}$ are expressed as functions of the original parameters of the Hamiltonian by means of w_0, w_1 and w_2.

Thereafter, the Boltzmann factor for effective spinless fermion model reads as

$$\tilde{w}_0 = 1, \quad \tilde{w}_1 = \mathrm{e}^{\beta\tilde{\mu}/2} = x, \quad \tilde{w}_2 = \mathrm{e}^{\beta\tilde{\mu}-\beta\tilde{V}} = x^2 y, \quad (46)$$

where $x = \exp(\beta\tilde{\mu}/2)$ and $y = \exp(-\beta\tilde{V})$.

We are interested in solving the effective spinless fermion without hoping term (also known as in atomic limit), to solve this effective model the transfer matrix method [34] will be used

$$\mathcal{T} = \begin{pmatrix} 1 & x \\ x & yx^2 \end{pmatrix}. \qquad (47)$$

It can be noted that the terms $\tilde{\mu}$ and $\tilde{V}$ can be obtained in a similar way as they were obtained for spin models. The eigenvalues of transfer matrix are given by $\lambda_{\pm} = \left(1 + yx^2 \pm \sqrt{(1-yx^2)^2 + 4x^2}\right)/2$. This result is exactly the same result to that obtained for the case of spinless diamond chain [16].

Using the largest eigenvalues λ_+ of the transfer matrix $\mathcal{T}$, we obtain the partition function per site of the model in terms of the effective spinless fermion model in atomic limit $\mathcal{Z} = f\mathcal{Z}_{eff}$, with $\mathcal{Z}_{eff} = \lambda_+$ and the partition function for effective spinless fermion without hopping term. The partition function per elementary cell, is expressed in terms of the Boltzmann factors for the spinless fermion model on tetrahedron chain, thus the partition function becomes

$$\mathcal{Z} = \frac{1}{2}\left(w_0 + w_2 + \sqrt{(w_0 - w_2)^2 + 4w_1^2}\right). \tag{48}$$

Once known the partition function of spinless fermion model on triangular plaquettes chain, it is possible to obtain the free energy by the relation $\Omega = -kT\ln\mathcal{Z}$. Therefore, we are ready to study several physical amounts such as entropy, specific heat, average energy and others.

V. THERMODYNAMICS

In this section, we discuss our most interesting results, using some relevant thermodynamic quantities that enable to reveal the competition between the possible ground states. Actually, in several works, many properties of the system are presented as a function of the chemical potential μ. Although from a theoretical point of view the chemical potential and particle density are conjugated variables, experimentally it is possible to manipulate in a controlled way, by varying the entering and outgoing particles to the system. Following the same procedure to that reference [16], to obtain explicitly the electron density per elementary cell, we take the derivative of free energy in relation to the chemical potential of spinless fermion on triangular plaquettes chain

$$\rho = -\left.\frac{\partial\Omega}{\partial\mu}\right|_{\beta} = 3\langle\mathbf{n}_a\rangle + \langle\mathbf{n}_d\rangle, \tag{49}$$

here we are assuming the exchange invariance of sites a, b and c.

The particle density of type d can be obtained from effective spinless fermion model, by the relation

$$\langle\mathbf{n}_d\rangle = \frac{1}{1 + \left(\frac{x}{\lambda_+ - 1}\right)^2}, \tag{50}$$

whereas the particle density for sites a, b, and c, can be obtained combining Eqs. (49) and (50), resulting in

$$\langle\mathbf{n}_a\rangle = \frac{\rho - \langle\mathbf{n}_d\rangle}{3}. \tag{51}$$

Before investigating the thermodynamical properties of the system, it is worth to observe the chemical potential dependence of the total electron density ρ, as displayed in Fig. 3(a) for fixed $t = 1$, $V = 1$ and $V_1 = 1$, and in Fig. 3(b) for fixed $t = 1$, $V = 1$ and $V_1 = 0.1$. At very low temperature, the model displays three distinct plateaus; for density $\rho = 1$, 2 and 3, besides the trivial empty particle ($\rho = 0$) and fully-filled particle ($\rho = 4$) states. Here and from now on we will consider all temperature dependence in unit of k_B for simplicity For $\mu = -2$, the density jumps from the trivial empty $\rho = 0$ to $\rho = 1$, where the plateau up to $\mu = 1$. Thereafter, the density jumps again to $\rho = 2$ and consequently remains roughly constant up to $\mu = 2$. The discontinuity for density $\rho = 2$ to $\rho = 3$ will be present for $\mu = 2$. Then the plateau remains until reaching $\mu = 5$, in which we have a final jump of the discontinuity reaching the density $\rho = 4$. Moreover, the thermal fluctuation smoothes the curves of particle density and for higher temperature just continuous crossovers are observed. The curves from different temperatures also cross roughly at a single point near the crossover from the particle density plateau to the saturation plateau.

Another important property to be discussed is the symmetry particle-hole described by Eq. (3) which will be satisfied, therefore, we find the following relation for the free energy,

$$\Omega(t,\, V,\, V_1) = \Omega(t,\, V,\, V_1 = V) + (3V_1 - 3V). \tag{52}$$

The chemical potential usually depends on the temperature, however at half-filled band electron density $\rho = 2$, the chemical potential becomes independent of the temperature, given simply by $\mu = \frac{3V}{2}$. If we look at the phase diagram displayed in Fig 3(a), the value $\mu = 1.5$ corresponds to the density $\rho = 2$. However, the total density of electron undergoes true transitions between these phases only at zero temperature, where in fact jumps emerge of discontinuity in the curves of density in certain critical points of the chemical potential (see Fig. 2). Quantum fluctuation, rather than thermal fluctuation, are responsible for such zero temperature phase transitions.

In Fig. 4 the temperature dependence of total density is shown for different values of the chemical potential μ. Thus, at $T = 0$, ρ leads to discrete values, as shown in Fig. 4, from where two significant situations can be explicitly calculated using Eq. (49), firstly, when $\mu = 1$, in the limit $T \to 0$, we obtain $\rho = 2 - \frac{\sqrt{5}}{5}$, while in the case $\mu = 2$, and $T \to 0$, the total density leads to $\rho = 2 + \frac{\sqrt{5}}{5}$. These values achieved are slightly different from that naive average in an unit cell, which could be $\rho = 1.5$ or $\rho = 2.5$ respectively. This difference is related to the frustration and in order to calculate the density ρ we need to calculate the average ρ in whole lattice instead of only an unit cell. Besides, from this plot we may also conclude the total particle density ($\rho = 2$, for $\mu = 1.5$) is independent of the temperature only at half-filled band.

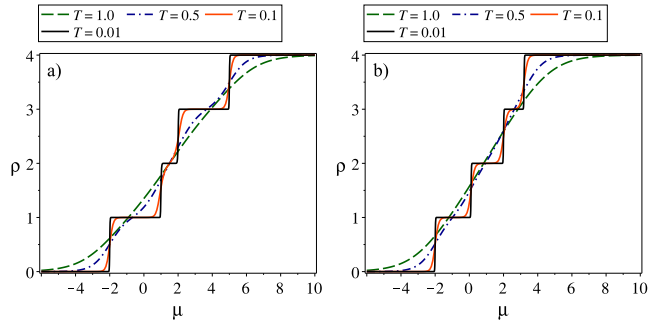

FIG. 3: (Color Online) Total density ρ as a function of chemical potential μ, for fixed values of the temperature and $t = 1.0$. (a) $V = V_1 = 1$. (b) $V = 1$ and $V_1 = 0.1$.

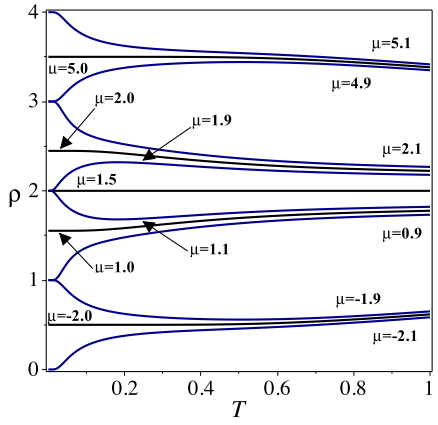

FIG. 4: (Color Online) Total density ρ as a function of the temperature T, for several values of chemical potential.

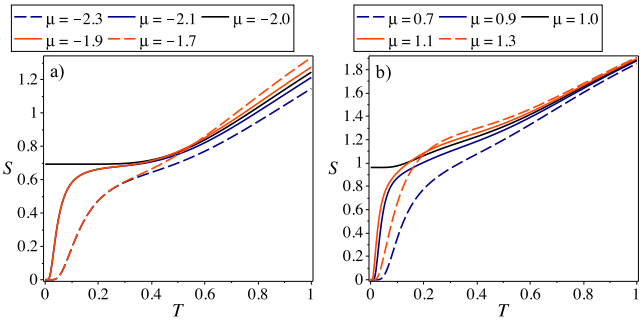

FIG. 5: (Color Online) Temperature dependence of the entropy for $t = 1.0$, $V = V_1 = 1.0$ and several values of the chemical potential. (a) $\mu = -2.3, -2.1, -2.0, -1.9, -1.7$ (b) $\mu = 0.7,\ 0.9,\ 1.0,\ 1.1,\ 1.3$.

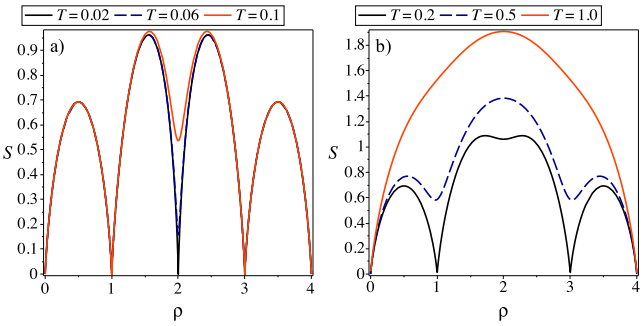

FIG. 6: (Color Online) Entropy as a function of the total density ρ for $t = 1.0$, $V = V_1 = 1.0$ and several values of the temperature (a) $T = 0.02,\ 0.06$ and 0.1; (b) $T = 0.2,\ 0.5$ and 1.0.

At this point, we will turn our attention to an investigation of the entropy. One can easily determine the expression for the entropy according to the general thermodynamic relation

$$S = -\left(\frac{\partial \Omega}{\partial T}\right)_{\mu}. \tag{53}$$

In Fig. 5, we report the temperature dependence of entropy S, for several chemical potential values, for fixed $t = 1$ and $V = V_1 = 1$. The behavior of the entropy around $\mu = -2.0$ are shown in Fig. 5(a), where the entropy takes the value $\ln(2)$ for $\mu = -2.0$, this is the so called residual entropy. Moreover, for $\mu = 5$, we have the same value of residual entropy. While, in Fig. 5 (b) the residual entropy has a different non-trivial value. To obtain explicitly the entropy we return to Eq. (53) and the limit $T \to 0$, the residual entropy results in $S = \ln(2) - \ln\left(3 - \sqrt{5}\right)$, for $\mu = 1$ and $\mu = 2$.

At zero temperature, the entropy is discontinuous at the transition boundary, signaling the first-order zero-temperature phase transition. However, at finite temperatures, the thermal fluctuations round off the discontinuity. The total density dependence of entropy are depicted in Fig. 6(a). At first, looking more closely in the low temperature limit, the degenerate state $F1$ and $F2$, corresponding to the region of half-filled band particle density ($\rho = 2$), are broken, as a consequence of the entropy increases rapidly. Meanwhile, when the temperature increases, the peaks are gradually merged into one, as shown in Fig. 6(b).

Another quantity to be plot is the entropy as a function of chemical potential, which exhibits a series of peaks that correspond to the residual entropy as displayed in Fig. 7. Explicitly, the entropy in phase transitions between $S0 \longleftrightarrow S1$ ($S3 \longleftrightarrow S4$) takes the value $\ln(2)$, certainly this factor comes from two different configurations for each phase, this generates an infinitely degenerated state at zero temperature. However, the transitions between $S1 \longleftrightarrow F1, F2$ ($F1, F2 \longleftrightarrow S3$) takes a non-trivial value of residual entropy $S = \ln(2) - \ln(3 - \sqrt{5})$, this factor again comes from two states, one of them non-degenerated and the other two-fold degenerated states, in the zero temperature limit. On the other hand, in Fig. 7 the behavior of entropy at very low temperatures in the neighborhood of the critical values of μ and how the residual entropy leads to the value discussed above in the limit $T = 0$.

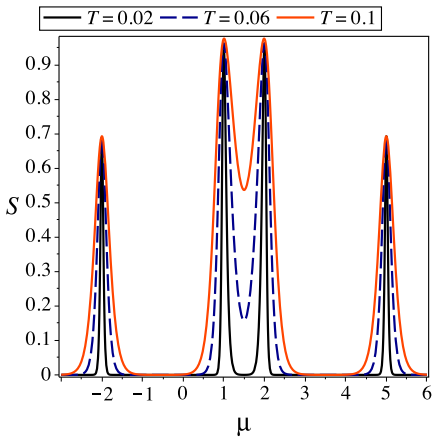

FIG. 7: (Color Online) Entropy as a function of the chemical potential μ with $t = 1.0$, $V = V_1 = 1.0$, in the low temperature limit.

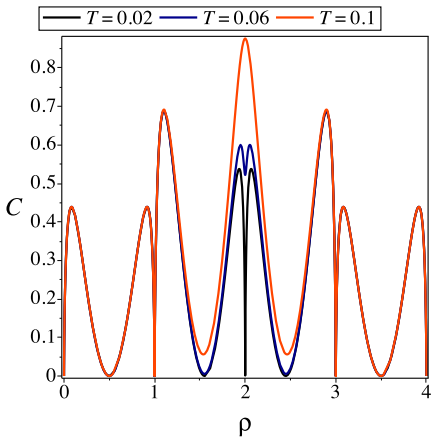

FIG. 9: (Color Online) Specific heat C as function of total density ρ for low values of the T, with $t = 1.0$ and $V = V_1 = 1.0$.

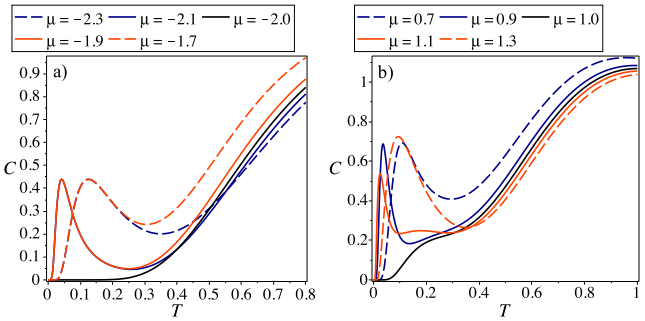

FIG. 8: (Color Online) Specific heat C is plotted as a function of the temperature T for $t = 1.0$, $V = V_1 = 1.0$ and different values of chemical potential. (a) $\mu = -2, 3, -2.1 - 2.0, -1.9, -1.7$. (b) $\mu = 0.7, 0.9, 1.0, 1.1, 1.3$.

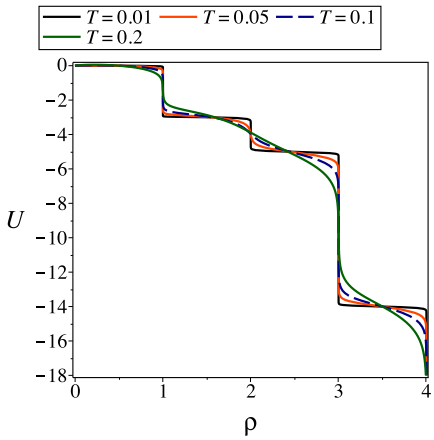

FIG. 10: (Color Online) Total density ρ dependence of the internal energy U, for low values of the temperature T , with $t = 1.0$, $V = V_1 = 1.0$.

A further quantity which is important for a better understanding of thermodynamics is the specific heat $C = -\beta\frac{\partial S}{\partial \beta}$, as shown in plots of the specific heat displayed in Fig. 8. Thus, for certain values of μ, the specific heat has two peaks: one standard maximum peak and another small peak in the lower temperature region. The maximum at low temperature is influenced by the phase transition between $S0$, $S1$, $F1$, $(F2)$, $S3$ and $S4$ states caused by thermal excitations and quantum fluctuations. One can see in Fig. 8, a series of peaks that appear in the curves at low temperatures, which are in agreement with the zero temperature phase transition, as illustrated in Fig. 2. When the chemical potential moves away from the critical point, the peak moves to a higher temperature region, roughly keeping its amplitude. While higher temperatures, the specific heat has a different behavior depending on the choice of μ, for example the one in Fig. 8 (a) for $\mu = -1.9$ and $\mu = -2.1$ at low temperatures the specific heat behavior is similar (blue and red solid line), whereas for $T \gtrsim 0.25$ the curvature behavior changes. In addition, for $\mu = 1.0$ and $\mu = 2.0$ see Fig. 8(b), the behavior of the specific heat becomes remarkably different.

In Fig. 9 we present the total density dependence of the specific heat for three values in the low temperature limit, $T = 0.02$, $T = 0.06$ and $T = 0.1$. In this Fig. 9, the corresponding plots exhibit four minimum values which are related to the phase transitions at zero temperature.

In Fig. 10 we illustrate the behavior of the internal energy $U = -\frac{\partial \ln Z}{\partial \beta}$ as a function of the electron density ρ, for different values of the temperature T. In the low temperature limit, we can observe several plateaus of internal energy that depend on the total particle density. The largest interval of almost constant internal energy configuration occurs between degenerate states $\mid S3\rangle$ and state $\mid S4\rangle$. Additionally, the smaller jump in the levels of internal energy configurations occur between states $\mid F1\rangle, (\mid F2\rangle)$ and $\mid S3\rangle$.

Finally, we conclude our analysis of the thermodynam-

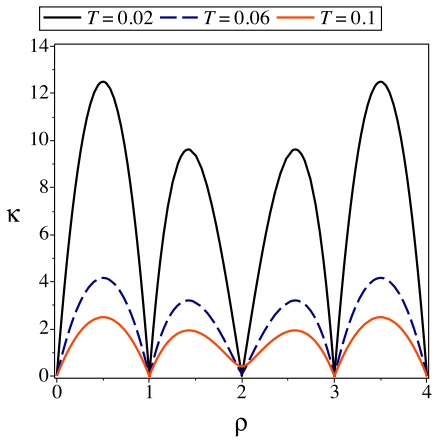

FIG. 11: (Color Online) Compressibility κ versus total electron density ρ for $t = 1.0$, $V = V_1 = 1$ and low values of the temperature T.

ics by exploring the compressibility $\kappa = \frac{\partial \rho}{\partial \mu}$ for $t = 1$, $V = V_1 = 1$ and different fixed temperatures shown in Fig. 11. The four peaks is a signature of the phase transitions discussed widely above. The structure of the peaks decreases when the temperature increases, in opposite to the peaks of entropy (see Figs. 6(a) and (b)) increase. This means that the system is stiffer close to integer particle density, as one can expect, since for those densities the system is well organized turning in a rigid structure. Due to the particle-hole symmetry, the compressibility is invariant under the transformation $\rho \to 4 - \rho$ or particle hole symmetry.

VI. CONCLUSIONS

In the present paper, we studied the spinless fermion on triangular plaquettes or tetrahedral chain with hopping term, repulsive Coulomb interactions particles between nearest-neighbor sites and chemical potential (acting only on triangle plaquette). This model has been exactly solved using the decoration transformation [26–29] and the transfer matrix [34] method. Within the framework of this exact analytical approach, the ground-state phase and the thermodynamics functions of the system were discussed in detail.

The phase diagrams are rather rich, four different states and one state two-fold degenerate ($|F1\rangle$ and $|F2\rangle$) are shown, changing from empty lattice of particles up to the saturated state of particles on the triangular plaquette or tetrahedral chain. We also observe that, there are frustrations between all phase boundaries. The region with particle density $\rho = 2$ is two-fold degenerated, so the boundary of this region becomes a frustrated state curve, with non-trivial residual entropy $S = \ln(2) - \ln(3 - \sqrt{5})$, whereas the other boundaries also become frustrated curves, but with trivial residual entropy $S = \ln(2)$, this factors comes when two phases becomes identical, producing an infinitely degenerated state, which leads to a frustrated state.

The existence of this non-trivial phenomenon has also been evidenced by temperature dependencies of the specific heat, as well as, a remarkable characteristic of the residual entropy remain constant until relatively high temperatures $T \approx 0.3$, for chemical potential $\mu = -2$ and 5. We also discuss the behavior of the particle density as a function of the chemical potential and temperature.

Finally, some other additional quantities were also considered, such as the internal energy and compressibility. Also we observe that, the behavior of the specific heat at low temperature is influenced by the interaction between thermal and quantum fluctuations.

Acknowledgments

O. Rojas and S. M. de Souza thank CNPq and FAPEMIG for partial financial support.

[1] R. R. Montenegro-Filho, and M. D. Coutinho-Filho, Phys. Rev. B **74**, 125117 (2006).
[2] F. Mancini, Eur. Phys. J. B **47**, 527 (2005); F. Mancini, and F. P. Mancini Phys. Rev. E **77**, 061120 (2008).
[3] J. Vidal, R. Mosseri, B. Doucot, Phys. Rev. Lett. **81**, 5888 (1998); J. Vidal et al., **85**, 3906 (2000); B. Doucot and J. Vidal, Phys. Rev. Lett. **88**, 227005 (2002).
[4] J. Rössler, and D. Mainemer, Cond. Matter Phys. **13**, 13704 (2010).
[5] W. Z. Wang, Phys. Rev. B **72**, 125116 (2005).
[6] Z. Gulácsi, A. Kampf, and D. Vollhardt, Phys. Rev. Lett. **99**, 026404 (2007).
[7] Z. Gulácsi, A. Kampf, and D. Vollhardt, Prog. Theor. Phys. Supp. **176**, 1 (2008).
[8] A. Honecker, S. Hu, R. Peters, and J. Ritcher, J. Phys.: Condens. Matter **23**, 164211 (2011).
[9] M. S. S. Pereira, F. A. B. F. de Moura, and M. L. Lyra, Phys. Rev. B **77**, 024402 (2008); Phys. Rev. B **79**, 054427 (2009).
[10] B. M. Lisnii, Ukrainian Journal of Physics **56**, 1237 (2011).
[11] O. Rojas, S. M. de Souza, V. Ohanyan and M. Khurshudyan, Phys. Rev. B **83** 094430 (2011).
[12] J. S. Valverde O. Rojas and S. M. de Souza, J. Phys. Condens. Matter. **20** 345208 (2008).
[13] L. Canova, J. Strecka, and M. Jascur, J. Phys.: Condens. Matter **18**, 4967 (2006).
[14] O. Rojas, M. Rojas, N. S. Ananikian, and S. M. de Souza Phys. Rev. A **86**, 042330 (2012); N. S. Ananikian, L. N. Ananikyan, L. A. Chakhmakhchyan, and O. Rojas, J. Phys.: Condens. Matter **24**, 256001 (2012).
[15] B. M. Lisnii, Low Temp. Phys. **37**, 296 (2011).

[16] O. Rojas, S. M. de Souza, Phys. Letts. A **375**, 1295 (2011).
[17] A. A. Lopes, R.G. Dias, Phys. Rev. B **84**, 085124 (2011).
[18] O. Rojas, S. M. de Souza and N. S. Ananikian, Phys. Rev. E 85, 061123 (2012).
[19] M. Mambrini, J. Trébosc, and F. Mila, Phys. Rev. B **59**, 13806 (1999).
[20] O. Rojas and F. C. Alcaraz Phys. Rev. B **67**,174401 (2003) .
[21] D. Antonosyan, S. Bellucci and V. Ohanyan, Phys. Rev. B **79**, 014432 (2009).
[22] V. Ohanyan, Phys. Atom. Nucl. **73**, 494 (2010).
[23] C. D. Batista, and B. S. Shastry, Phys. Rev. Lett. **91**, 116401 (2003).
[24] M. Maksymenko, O. Derzhko, and J. Richter, Eur. Phys. Journ. B **84**, 397 (2011) .
[25] J. Sznajd and Klaus W. Becker, J. Phys. Condens. Matter **17**, 7359 (2005).
[26] I. Syozi, Prog. Theor. Phys. **6**, 341 (1951) ; *Phase transition and Critical phenomena*, C. Domb and M. S. Green (Academic, New York, 1972), Vol. 1.
[27] M. E. Fisher, Phys. Rev. **113**, 969 (1959).
[28] O. Rojas, J. S. Valverde and S. M. de Souza, Physica A **388**, 1419 (2009); O. Rojas and S. M. de Souza, J. Phys. A: Math. Theor. **44**, 245001 (2011).
[29] J. Strecka, Phys. Lett. A **374**, 3718 (2010).
[30] L. Canova, and J. Strecka, T. Lucivjansky, J. Phys. Condens. Matter. **21**, 392201 (2009).
[31] M. Jascur, and J. Strecka, J. Magn. Magn. Matter **272**, 984 (2004).
[32] L. Canova, J. Strecka and M. Jascur, J. Phys. Condens. Matter. **18**, 4967 (2006).
[33] S. Belluci and V. Ohanyan, Eur. Phys. J. B Phys. Rev. B **75**, 531 (2010).
[34] R. J. Baxter, *Exactly solved models in statistical mechanics,* Academic Press, (1982).